Electrode-Electrolyte Compatibility in Solid-Oxide Fuel Cells: Investigation of the LSM-LNC interface with X-ray Microspectroscopy

Francesco Giannici[§,*], Giovanna Canu[$], Marianna Gambino[§], Alessandro Longo[£], Murielle Salomé[^], Massimo Viviani[$], and Antonino Martorana[§]

§ Dipartimento di Fisica e Chimica, Università di Palermo, Viale delle Scienze, I-90128 Palermo, Italy

$ Istituto per l'Energetica e le Interfasi (CNR-IENI), Consiglio Nazionale delle Ricerche, Via De Marini 6, I-16149 Genova, Italy

£ Istituto per lo Studio dei Materiali Nanostrutturati (CNR-ISMN), Consiglio Nazionale delle Ricerche, Via La Malfa 153, I-90146 Palermo, Italy

^ European Synchrotron Radiation Facility, F-38043 Grenoble Cedex 9, France

Solid-oxide fuel cells (SOFCs) are at the forefront of energy materials research, representing the most efficient way to convert a wide range of fuels to electrical energy. The research efforts have been mainly directed at the development and characterization of new materials, as reported in a number of recent reviews on these topics.[1-4] The structural and chemical compatibility between electrodes and electrolytes is a critical issue: the materials should display similar thermal expansion coefficients, and most importantly they should minimize the interdiffusion of chemical species at the interface.[1,5] The formation of insulating phases due to cation diffusion is usually investigated by means of X-ray Diffraction (XRD), to detect the growth of crystalline phases in powder mixtures treated at high temperatures.[6-10] From the microchemical point of view, the information on the extent of cation interdiffusion is obtained with scanning electron microscopy/energy-dispersive spectroscopy (SEM/EDS) on cross-sections of the electrode-electrolyte assembly.[11] In some cases, electron microspectroscopy has also been used to elucidate the mechanisms of interdiffusion and the oxidation state of cations at the phase boundary between LSM/YSZ, LSCF/GDC and NiO/GDC.[12-15] Oxide ion-conducting SOFCs are currently reliable devices, the main goal of the research activity being a lower operating temperature,[2] while various problems linked to chemical stability, grain boundary resistance and sinterability have stifled until now the technology of proton-conducting SOFCs (PC-SOFCs). Despite these problems, the prospected advantages in terms of fuel management with respect to both polymer membranes and oxide-ion conductors strongly motivate the efforts to seek new electrolyte materials and suitable electrodes for PC-SOFCs.[8,16-18]

Doped cerate and zirconate perovskites have been proposed as proton conducting oxides in the early 1980s, and they have dominated the research on PC-SOFCs ever since.[19-22] To overcome the long-standing issues regarding sinterability, phase stability and chemical resistance to CO_2, $LaNbO_4$ was proposed as an alternative to perovskite compounds for use in PC-SOFCs.[16] In fact, $LaNbO_4$ can be regarded as the major breakthrough in the field of proton SOFC in the last decade, sparking extensive research efforts as what concerns the defect chemistry, microstructure, phase stability and chemical compatibility with a variety of electrode materials.[8-11] The defect chemistry of $LaNbO_4$ involves doping of the La^{3+} site with a divalent cation (usually Ca^{2+}), to generate oxygen vacancies which react with moisture yielding protonic defects. The overall doping reaction leading to the formation of charge carriers in the electrolyte is:

$$2CaO + 2La_{La}^{X} + H_2O + 2O_O^{X} \rightarrow 2OH_O^{\cdot} + 2Ca_{La}' + La_2O_3$$

To achieve useful FC performances, the modest proton conductivity (~0.6 mS/cm for 1% Ca-doped $LaNbO_4$ at 700 °C) requires that the electrolyte thickness is brought down to a few micrometers.[16] Moreover, taking into account that the poor solubility of dopants in $LaNbO_4$ (up to 2 mol%) limits the concentration of protonic defects that can be introduced in the structure, it is evident that the fabrication of electrolyte-electrode assembly with good stability at operative conditions and limited dopants interdiffusion is of the utmost importance for SOFC devices based on $LaNbO_4$. In this respect, the cathode-electrolyte couple (lanthanum strontium manganite)-(calcium-doped lanthanum niobate) (LSM-LNC) was reported to present good chemical compatibility, and composites of the two materials showed mixed electronic/protonic conductivity.[10-11,23]

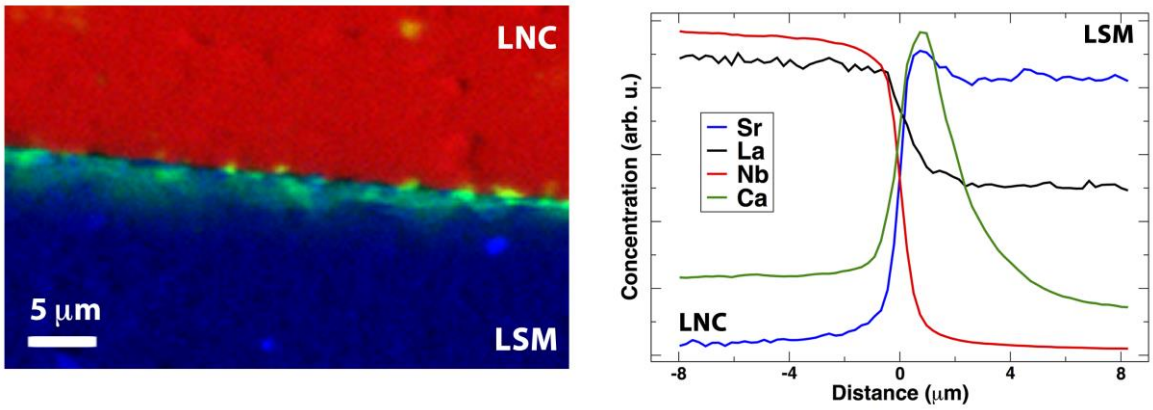

Figure 1. Sample A. Left: concentration map from microXRF data at the La L_3-edge: Nb in red, Ca in green, Sr in blue; Right: concentration profiles of Sr, La, Nb and Ca measured across the boundary between LSM and LNC phases, rescaled for clarity.

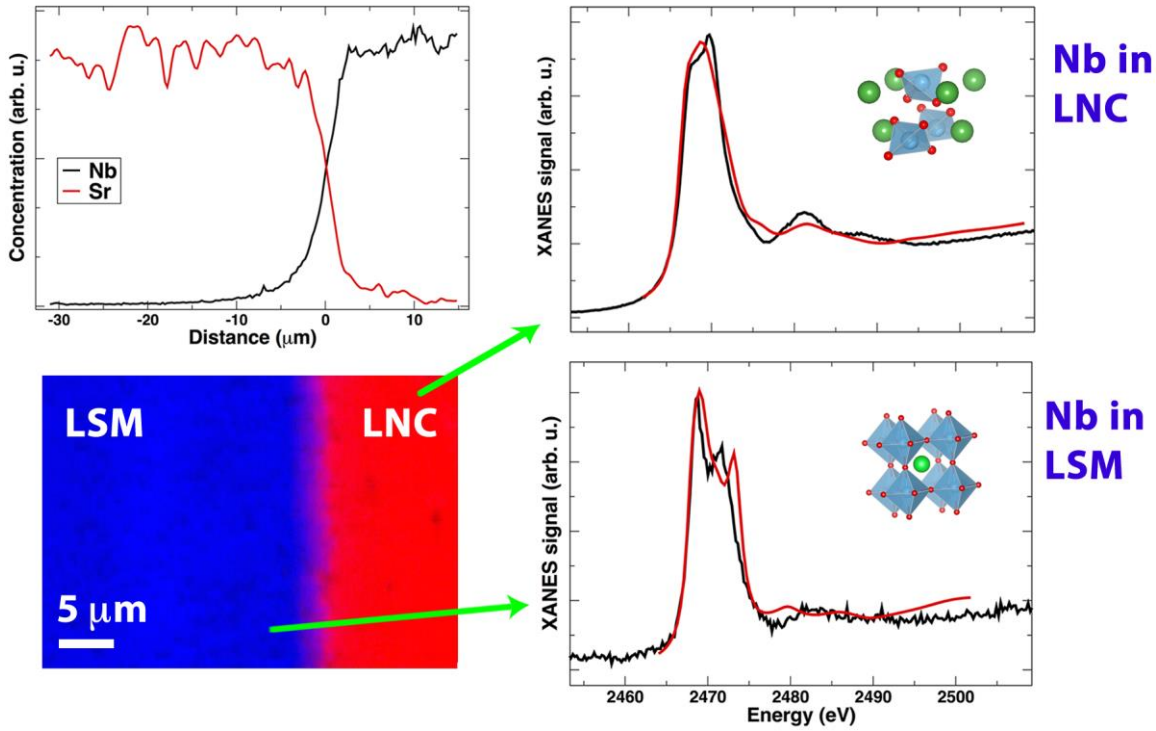

Figure 2. Sample B. Left panel, bottom: Concentration map of Nb from microXRF data at the Nb L_3-edge: lowest (blue) to highest (red). Left panel, top: Concentration profiles of Nb and Sr in the map, rescaled for clarity. Right panel, bottom: experimental Nb L_3-edge microXANES spectrum from the LSM region, and simulated signal for Nb placed in the B-site of the perovskite LSM structure. Right panel, top: experimental Nb L_3-edge microXANES spectrum from the LNC region, and simulated signal for Nb placed in the monoclinic LNC structure. In the right panels, the experimental data are plotted in black, and the simulations in red.

In this communication, we report on the LSM-LNC microchemical compatibility investigated by X-ray microspectroscopy. The bilayers were assembled by pressing together a dense $La_{0.98}Ca_{0.02}NbO_{4-x}$ electrolyte pellet (LNC) and $La_{0.8}Sr_{0.2}MnO_{3-x}$ (LSM) cathode powder. The bilayers was then heat-treated at 1150 °C for either 12 h (sample A) or 36 h (sample B); another sample was treated at 1250 °C for 72 h (sample C). All samples were embedded in epoxy resin, cross-cut and polished to expose the interlayer surface. A focused monochromatic X-ray microbeam from a synchrotron undulator source was used to scan the LSM-LNC interface cross section and to excite the fluorescence radiation from the sample. The L_3-edge of La (5.5 keV) is ideally suited for calcium determination, as it gives high sensitivity (Ca K-edge at 4.0 keV), and no overlap between the K_α lines of Ca and the L lines of La. In this way, the distribution of Ca^{2+} throughout the interface of the annealed LSM-LNC bilayers is quantitatively determined. For sample A, the color map reported in Figure 1 gives a graphical insight of the diffusion of Ca^{2+} towards the cathode: after a sharp accumulation, the further diffusion toward the innermost layers of the cathode

is evidenced by the Ca concentration profile, which decreases smoothly in the LSM region. The elemental composition in three regions is reported in Table 1. Microbeam Extended X-ray Absorption Fine Structure and X-ray Absorption Near-edge Structure (microEXAFS and microXANES) spectra were also collected on the Nb L_3-edge and Mn K-edge, giving information on the fate of different cations.

The microspectroscopy experiment was carried out at the SXM-II endstation at ID21 beamline of ESRF.[24] The monochromatic beam is focused down to a submicron probe with Kirkpatrick-Baez mirrors: this is used to scan the sample in two dimensions to produce a XRF map. All data reduction and XRF analysis was performed with PyMca.[25] The X-ray beam was tuned to Nb L_3-edge, La L_3-edge, and Mn K-edge, and focused to 0.4 x 0.7 μm^2 with a flux of about 10^{10} photons/s. The high flux ensures high sensitivity and precision, and low detection limits in the XRF analysis. At the beam energy used (2.5 – 7 keV) the attenuation length is around 1-5 micron, which is large enough so that the results are not critically affected by the roughness of the surface. Using an X-ray probe also ensures that there are no aberrations due to the electrostatic charging of insulating samples. In addition to microXRF, microXANES and microEXAFS spectra were also recorded in selected points, by varying the X-ray beam energy around the absorption edge of the element of interest.

In general, no clear formation of a secondary phase can be observed at the interlayer of samples A-C (see figure 1). Actually, the drift of Ca^{2+} in LSM could be enhanced by the recognized structural flexibility of perovskite oxides, which are able to compensate for changes in composition by tilting and deformation of the BO_6 octahedra. On the other hand, the doping of $LaNbO_4$ is much less favoured, with fairly low solubility limits on both the La and Nb sites. Further insight on the structural details of Nb and Mn atomic environment comes from the analysis of microspectroscopy data. The L_3-edge XANES features of Nb (2.4 keV) are very sensitive to the coordination environment and oxidation state of niobium, thanks to the low lifetime broadening. The relevant data and simulations for sample B are shown in Figure 2. The spectra can be modeled satisfactorily in regions of the map corresponding to LNC (where Nb^{5+} is placed in a tetrahedral environment), and also inside LSM, where Nb is detected at about 2.5% at 5 µm from the interphase. The analysis of XANES features demonstrates a coordination change from tetrahedral to octahedral in the LSM region, strongly suggesting that Nb^{5+} is incorporated in the perovskite B-site. Because of its higher charge, Nb^{5+} shows a relatively slow diffusion compared to other cations, and a shorter treatment time (sample A) does not induce a significant incorporation of niobium in the perovskite structure of the cathode.

The microXANES and microEXAFS spectra at the Mn K-edge provide indirect evidence on the fate of the Ca^{2+} ions that diffuse out of the LNC electrolyte phase.

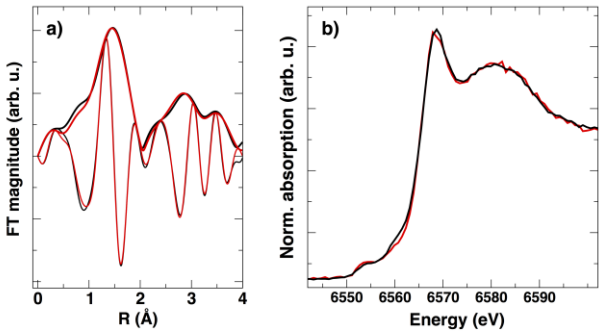

Figure 3. Sample C. a) Mn K-edge microEXAFS at the LNC-LSM interface: experimental data (black) and fit (red). b) experimental Mn K-edge microXANES at the LNC-LSM interface (black) and in bulk LSM (red).

We chose the extreme treatment conditions of sample C (72 h at 1250 °C) to cause a sizable ingress of calcium in the LSM phase, and to obtain a substantial effect on the local environment of Mn. The microXRF analysis at the LNC-LSM interface gives a composition $La_{0.7}Sr_{0.2}Ca_{0.1}MnO_3$ and, on the same spot, simulation of the Mn microEXAFS signal with the Sr and Ca contributions weighed according to the microXRF analysis gives a very satisfactory fit (Figure 3). So, taking into account that La, Sr and Ca, are very well distinguishable when fitting EXAFS data, it can be concluded that Ca^{2+} drifts into the perovskite A-site of LSM. The incorporation of Ca in the LSM A-site is not surprising, as this particular composition falls in a single phase region of the $LaMnO_3$-$CaMnO_3$-$SrMnO_3$ ternary diagram.[26] The changes in the microXANES spectra at the LNC-LSM interface and in the LSM bulk confirm that the Mn environment is modified by calcium (Figure 3b). Therefore, it seems plausible that the formation of a perovskite phase like (La,Ca,Sr)MnO_3 provides the driving force for the diffusion of calcium out of LNC. In fact, a recent report on the cation segregation of $LaMnO_3$ surfaces proposed that doping with Ca results in the highest stability, compared to Ba and Sr.[27] Using synchrotron X-ray microspectroscopy to scan the LSM-LNC interface, we have demonstrated that an impressive Ca^{2+} drift towards the cathode takes place, whose charge is likely balanced by counterdiffusion of La^{3+} and consequent annihilation of protonic defects. Even if no evidence of undesired interfacial phases have been detected, the Ca^{2+} dopant is depleted throughout a region of LNC several micrometers wide (comparable to the actual thickness of a thin electrolyte membrane): this clearly produces a decrease of charge carriers in the electrolyte and likely impairs the conductivity. This depletion is not compensated by an equal counterdiffusion of strontium from the cathode towards the electrode. The validity of such considerations goes beyond this particular case, as calcium is also able to occupy the A-site in perovskites with Fe, Cr, or Co, which are present in almost all candidate materials for cathodes.[28,29]

Table 1. Elemental composition (weight %) of three regions of sample A.

Element	Region #1 (LSM)	Region #2 (interface)	Region #3 (LNC)	LSM (nominal)	LNC (nominal)
La	47.71	46.78	46.66	47.98	46.33
Sr	8.765	8.176	0.071	7.56	0
Ca	0.0407	0.3425	0.1494	0	0.27
Nb	0.2822	1.775	31.2637	0	31.62
Mn[a)]	23.121	22.584	0.18	23.72	0

[a)] Manganese content is determined by difference. Such estimation is confirmed by the microXRF analysis at the Mn K-edge on the same regions (see Supporting Information). Regions 1-3 are depicted in Figure S4.

This poses a significant challenge for the suitability of the electrolyte/cathode interface in PC-SOFCs based on LNC, especially when the electrolyte is present as a thin film, and it could also explain the low performance of the LSCM-LCN cathode-electrolyte pair reported recently.[10] As the doping level attainable in LNC is already low, the dopant diffusion towards the electrodes would dramatically deplete the charge carrier density.

Beside the specific interest for the development of feasible PC-SOFC devices, the X-ray microspectroscopy approach described here is proposed as a useful structural tool, complementary to electrochemical characterization, for the investigation of the compatibility between SOFC materials. The atomic diffusion, not necessarily giving rise to the formation of secondary phases, is a further critical point to consider in the design and fabrication of SOFCs.

ASSOCIATED CONTENT

Supporting Information. Experimental details. This material is available free of charge via the Internet at http://pubs.acs.org.

AUTHOR INFORMATION

Corresponding Author

* E-mail: francesco.giannici@unipa.it

ACKNOWLEDGMENT

We acknowledge funding through the MIUR project Futuro in Ricerca INCYPIT (RBFR12CQP5). We acknowledge the ESRF for provision of beamtime, Dr. C. Tealdi (University of Pavia) for assistance in sample preparation and Dr. V. Buscaglia (IENI-CNR) for useful discussions.

REFERENCES

(1) Tsipis, E. V.; Kharton, V. V. *J. Solid State Electrochem.* **2008**, *12*, 1367.

(2) Wachsman, E. D.; Lee, K. T. *Science* **2011**, *334*, 935.

(3) Shao, Z.; Zhou, W.; Zhu, Z. *Prog. Mater. Sci.* **2012**, *57*, 804.

(4) Cowin, P. I.; Petit, C. T. G.; Lan, R.; Irvine, J. T. S.; Tao, S. *Adv. Energy Mater.* **2011**, *1*, 314.

(5) Taroco, H. A.; Santos, J. A. F.; Domingues, R. Z.; Matencio, T. in *Advances in Ceramics: Synthesis and Characterization, Processing and Specific Applications*, (Ed. C. Sikalidis), InTech, 2011.

(6) Wiik, K.; Schmidt, C. R.; Faaland, S.; Shamsili, S.; Einarsrud, M.-A.; Grande, T. *J. Am. Ceram. Soc.* **1999**, *82*, 721.

(7) Stochniol, G.; Syskakis, E.; Naoumidis, A. *J. Am. Ceram. Soc.* **1995**, *78*, 929.

(8) Tolchard, J. R.; Lein, H. L.; Grande, T. *J. Eur. Ceram. Soc.* **2009**, *29*, 2823.

(9) Magrasó, A.; Fontaine, M.-L. *J. Power Sources* **2011**, *196*, 10183.

(10) Magrasó, A.; Fontaine, M.-L.; Bredesen, R.; Haugsrud, R.; Norby, T. *Solid State Ionics* **2014**, *262*, 382.

(11) Kravchyk, K. V.; Quarez, E.; Solìs, C.; Serra, J. M.; Joubert, O. *Int. J. Hydrogen Energ.* **2011**, *36*, 1305.

(12) Backhaus-Ricoult, M. *Solid State Ionics* **2006**, *177*, 2195.

(13) Backhaus-Ricoult, M.; Adib, K.; St.Clair, T.; Luerssen, B.; Gregoratti, L.; Barinov, A. *Solid State Ionics* **2008**, *179*, 891.

(14) Li, Z.-P. Toshiyuk, M. Auchterlonie, G. J. Zou, J. Drennan, J. *ACS Appl. Mater. Interfaces* **2011**, *3*, 2772.

(15) Li, Z.-P.; Toshiyuk, M.; Auchterlonie, G. J.; Guo, Y.; Zou, J.; Drennan, J.; Miyayama, M. *J. Phys. Chem. C* **2011**, *115*, 6877.

(16) Haugsrud, R.; Norby, T. *Nature Mater.* **2006**, *5*, 193.

(17) Zayas-Rey, M. J.; dos Santos-Gómez, L.; Marrero-López, D.; León-Reina, L.; Canales-Vázquez, J.; Aranda, M. A. G.; Losilla, E. R. *Chem. Mater.* **2013**, *25*, 448.

(18) Magrasó, A.; Fontaine, M.-L.; Haugsrud, R.; Norby, T. *J. Electrochem. Soc.* **2014**, *161*, F373.

(19) Kreuer, K.-D. *Annu. Rev. Mater. Res.* **2003**, *33*, 333-359.

(20) Giannici, F.; Longo, A.; Balerna, A.; Kreuer, K.-D.; Martorana, A. *Chem. Mater.* **2009**, *21*, 2641.

(21) Giannici, F.; Longo, A.; Kreuer, K.-D.; Balerna, A.; Martorana, A. *Solid State Ionics* **2010**, *181*, 122.

(22) Giannici, F.; Shirpour, M.; Longo, A.; Martorana, A.; Merkle, R.; Maier, J. *Chem. Mater.* **2011**, *23*, 2994.

(23) Magrasó, A.; Fontaine, M.-L.; Larring, Y.; Bredesen, R.; Syvertsen, G. E.; Lein, H. L.; Grande, T.; Huse, M.; Strandbakke, R.; Haugsrud, R.; Norby, T. *Fuel Cells* **2011**, *11*, 17.

(24) Salomé, M.; Cotte, M.; Baker, R.; Barrett, R.; Benseny-Cases, N.; Berruyer, G.; Bugnazet, D.; Castillo-Michel, H.; Cornu, C.; Fayard, B.; Gagliardini, E.; Hino, R.; Morse, J.; Papillon, E.; Pouyet, E.; Rivard, C.; Solé, V. A.; Susini, J.; Veronesi, G. *J. Phys. Conf. Series* **2013**, *425*, 182004-1.

(25) Solé, V. A.; Papillon, E.; Cotte, M.; Walter, P.; Susini J. *Spectrochim. Acta B* **2007**, *62*, 63.

(26) Majewski, P.; Epple, L.; Aldinger, F. *J. Am. Ceram. Soc.* **2000**, *83*, 1513.

(27) Lee, W.; Han, J. W.; Chen, Y.; Cai, Z.; Yildiz, B. *J. Am. Chem. Soc.* **2013**, *135*, 7909.

(28) Woodward, P. M.; Cox, D. E.; Moshopoulou, E.; Sleight, A. W.; Morimoto, S. *Phys. Rev. B* **2000**, *62*, 844.

(29) Koc, R.; Anderson, H. U. *J. Mater. Sci.* **1992**, *27*, 5477.